# ChemComm

Accepted Manuscript


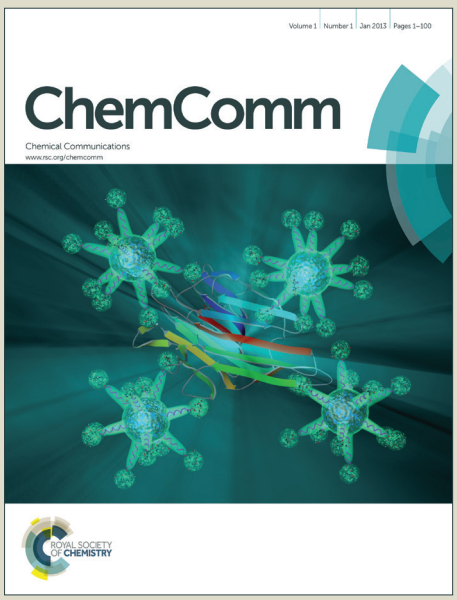





ROYAL SOCIETY OF CHEMISTRY

www.rsc.org/chemcomm

Journal Name

RSCPublishing

COMMUNICATION

# Hole Transporting Oligothiophene for Planar Perovskite Solar Cells with Improved Stability

Cite this: DOI: 10.1039/x0xx00000x

Lingling Zheng,[a] Yao-Hsien Chung,[a] Yingzhuang Ma, [a] Lipei Zhang,[a] Lixin Xiao,[a,b,*] Zhijian Chen,[a,b] Shufeng Wang,[a,b] Bo Qu,[a,b] and Qihuang Gong[a]

Received ooth January 2012,
Accepted ooth January 2012

DOI: 10.1039/x0xx00000x

www.rsc.org/

**An oligothiophene derivative named DR3TBDTT with high hydrophobicity was synthesized and functioned as the hole transporting material without ion additive. 8.8% of power conversion efficiency was obtained for $CH_3NH_3PbI_{3-x}Cl_x$ based planar solar cells with improved stability, compared to devices using Li-TFSI doped spiro-MeOTAD.**

Recently, organic-inorganic hybrid perovskite materials have rapidly developed and attracted significant research interest due to its excellent absorption and transporting properties. $CH_3NH_3PbI_3$ and $CH_3NH_3PbBr_3$ were firstly used as the light absorbers in liquid dye-sensitized solar cells by Miyasaka et al.[1] Benefiting from the solid-state hole transporting material (HTM) of 2,2′,7,7′-tetrakis(*N*,*N*-di-*p*-methoxyphenylamine)-9,9′-spirobifluorene (spiro-MeOTAD), much higher power conversion efficiencies (PCEs) have been achieved in solid-state cells than those of liquid ones,[2-7] and exceeded 15% in a short term.[8-13] N. J. Jeon et al changed *p*-OMe substituents of the conventional spiro-MeOTAD, 16.7% of PCE was obtained using the derivative with *o*-OMe substituents for mesostructured perovskite solar cells.[13] Owing to the difficulty on the purification of spiro-MeOTAD, many other triphenylamine derivatives were reported as the HTMs.[14-20] However, almost all these HTMs reported for solution-process perovskite solar cells needed the addition of ion additives, e.g., lithium bis(trifluoromethylsulfonyl)imide (Li-TFSI) with 4-*tert*-butylpyridine (*t*BP) to achieve improved hole mobility and device performance.[13-27] Few HTM in its pristine form can compete with additive doped spiro-MeOTAD for perovskite solar cells. P. Qin et al reported a branched conjugated HTM working alone for meso-structured perovskite solar cells with a high PCE of 12.8%.[28] The use of Li-TFSI should be avoided, because it will not only increase the costs, but also seriously deteriorate the stability of the perovskite due to its high hydroscopicity leading to the decomposition of perovskite.[29,30]

Oligothiophenes containing a backbone structure of a benzodithiophene (BDT) unit as the central block and ethylrhodanine as the end group (DR3TBDTT) were highly efficient donors with a high hole mobility of $10^{-4}$ $cm^2V^{-1}s^{-1}$ in the bulk heterojuction solar cells.[31-33] In this article, we modified the alkyl groups of DR3TBDTT to obtain an low-lying energy level of highest occupied molecular orbital (HOMO) (5.39 eV), matching with the HOMO of perovskite (5.43 eV) (**Figure 1**). As a result, the highest PCE of 8.8% was achieved using DR3TBDTT added by a small amount of polydimethylsiloxane (PDMS) as the HTM without the ion additive, comparable to 8.9% for spiro-MeOTAD doped with Li-TFSI and *t*BP. Moreover, the resultant oligothiophene possessed a high hydrophobicity with a water contact angle of 107.4°, which can be expected to prevent water penetration. So, the perovskite in devices without the hydroscopic Li-TFSI showed an improved stability resulting from the moisture resistance of oligothiophene. This work provides an alternative candidate of HTM dispensed with the ion additive for stable perovskite solar cells.

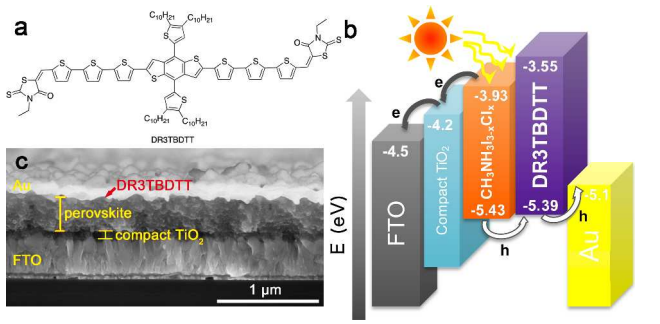


Figure 1. a) The chemical structure of DR3TBDTT. b) The relative energy level diagram of perovskite solar cell. c) Cross-sectional SEM image of the planar perovskite solar cell using DR3TBDTT as the HTM.

The solution and thin-film UV-vis absorption spectra of DR3TBDTT are presented in **Figure S1a†.** DR3TBDTT in diluted chloroform solution exhibited an absorption peak at 528 nm. The film spectrum showed two absorption peaks at 588 nm and 614 nm, one of which is a vibronic shoulder, corresponding to the $\pi$-orbital overlap between the molecule backbones.[31-33] The optical band gap was estimated as 1.84 eV by the absorption onset of the film. HOMO energy level was

measured by photoelectron spectroscopy as 5.39 eV (**Figure S2**†), only 0.04 eV higher than the HOMO of $CH_3NH_3PbI_{3-x}Cl_x$, indicating an extreme low energy barrier for hole transporting. Density functional theory (DFT) calculations showed the HOMO of DR3TBDTT was mainly located at the BDT unit, and its LUMO was mainly located at ethylrhodanine of both ends, revealing a acceptor-donor-acceptor (A-D-A) backbone structure (**Figure S1b**†). The calculated HOMO energy level was 5.25 eV, close to the experimental result. Thermogravimetric analysis (TGA) and differential scanning calorimetry (DSC) analysis showed excellent stability of DR3TBDTT, with a high glass transition temperature of 224 °C and decomposition temperature of 398 °C (**Figure S3**†).

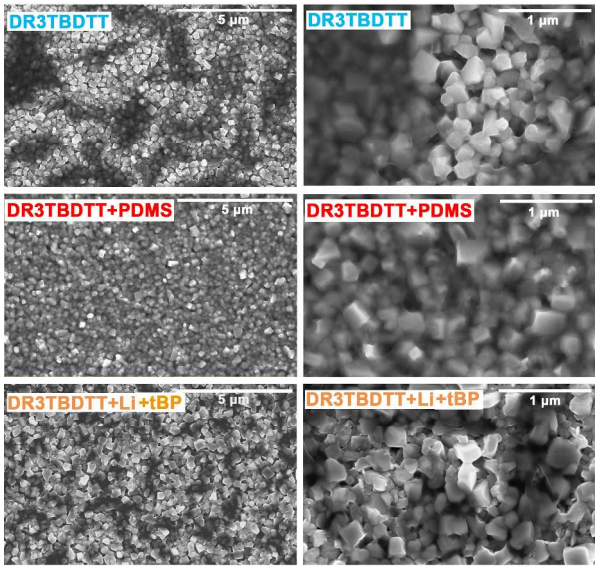


**Figure 2.** Top-view SEM images of perovskite layers covered by DR3TBDTT based HTMs (scale bar=5 μm and 1 μm).

To test the performance of DR3TBDTT, planar perovskite solar cells based on the structure of FTO/compact $TiO_2$/$CH_3NH_3PbI_{3-x}Cl_x$/HTM/Au were fabricated (**Figure 1**). A 350 nm thick $CH_3NH_3PbI_{3-x}Cl_x$ layer was fabricated by sequential deposition, using a mixture of $PbI_2$/$PbCl_2$ as the precursor according to our previous report.[34,35] The HTM layers were deposited by spin-coating. Besides using DR3TBDTT alone, we blended it with widely-used flow agent of PDMS to improve the morphology.[31,32,36] The influences of the conventional additive Li-TFSI and *t*BP on the performance and stability were also studied.

The scanning electron microscope (SEM) images were employed to observe the morphology of the HTM on the perovskite layer (**Figure 2**). All the relative elements can be observed in the respective energy dispersive spectra (EDS) (**Figure S4**†). From a solution of DR3TBDTT, the perovskite layer was only partially covered by HTM, probably due to the much larger surface tension of the solution than the surface energy of the perovskite,[36] which made it extremely difficult to form a continuous and uniform film on perovskite layer with a roughness of tens of nanometers.[4,35] With the aid of 0.1 mg/ml PDMS, full coverage on highly textured surface of perovskite was obtained, since the difference of the surface tension and the defects of the film could be eliminated by its low surface tension and high viscosity.[36] The introduction of Li-TFSI and *t*BP into DR3TBDTT solution led to a decreased coverage, appearing as the smaller domains of HTM on the perovskite. The HTM-coated perovskite films showed additional absorption in 500-670 nm consistent with the absorption of DR3TBDTT, and slightly higher absorption for film containing PDMS in this region also indicated more adhesion of HTM as shown in the SEM images (**Figure S5**†).

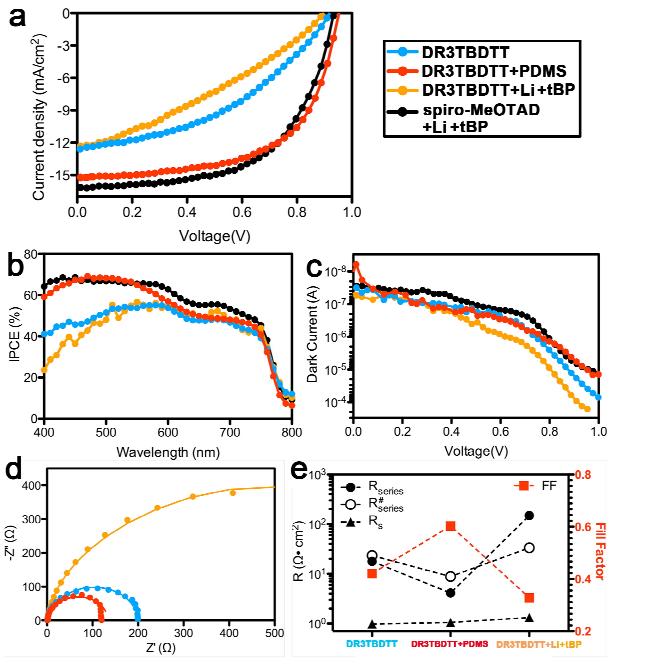


**Figure 3.** a) *J-V* curves, b) IPCE, and c) the dark current of the planar perovskite solar cells with different HTMs. d) Nyquist plots and the fitting line of perovskite solar cells in the perovskite/Au interface under the dark at respective $V_{oc}$. e) $R_s$ and $R_{series}$ obtained from EIS analysis compared to $R_{series}^{\#}$ and FF deduced from the *J-V* curves.

80 nm thick Au was thermally evaporated under vacuum on the HTMs as the cathode. As a comparison, devices containing widely used spiro-MeOTAD+Li+tBP as the HTM were also fabricated. The performance of each device under 100 mW $cm^{-2}$ simulated AM1.5G irradiation are shown in **Figure 3a** and listed in **Table S1**†. The PCE of the device with DR3TBDTT as HTM was 4.9%, with a low short-circuit current ($J_{sc}$) of 12.6 mA $cm^{-2}$ and a low fill factor (*FF*) of 0.42. By using DR3TBDTT+PDMS as the HTM, the performance improved significantly with a PCE of 8.8%, a $J_{sc}$ of 15.3 mA $cm^{-2}$, a *FF* of 0.60 and a open circuit voltage ($V_{oc}$) of 0.95 V, comparable to 8.9% PCE for spiro-MeOTAD+Li+tBP based device with a $V_{oc}$ of 0.93 V. A higher $V_{oc}$ of DR3TBDTT+PDMS device attributed to the deeper HOMO energy level (5.39 eV) of DR3TBDTT than that of spiro-MeOTAD (5.22 eV).[14] But the very close HOMO between DR3TBDTT and perovskite is unfavorably for charge transfer, resulting in the lower $J_{sc}$. Devices with DR3TBDTT+Li+tBP showed the poorest performance, especially on $V_{oc}$ and *FF*. As **Figure 3c** shown, at higher forward bias, the dark current increased from DR3TBDTT+PDMS to DR3TBDTT and to DR3TBDTT+Li+tBP based device, illustrating increased recombination leading to decreased $V_{oc}$.[37,38] As a result, the 0.17 eV HOMO level shift wasn't reflected in the extra $V_{oc}$ for the devices based on DR3TBDTT and DR3TBDTT+Li+tBP. The incident photon to current conversion efficiency (IPCE) (**Figure 3b**) showed the same shapes for all devices,

suggesting the absorption of the very thin DR3TBDTT has a negligible effect on the solar cells.[14,15] The integrated $J_{sc}$ calculated from the IPCE are well matched with the $J_{sc}$ from *J-V* curves.

Electrochemical impedance spectra (EIS) were employed to explain the significant difference of *FF* and the relations with the morphology of the HTM. The high-intermediate frequency arcs are shown in **Figure 3d**, respecting two individual processes, corresponding to the charge-transport resistance of Au/HTM interface and overlapping partially with the resistance in the HTM.[37-41] We fitted the high frequency feature with a parallel R-C circuit. The series resistance ($R_s$) can be obtained from the intersections of these arcs, corresponding to the resistance of the conducting glass, contacts and wires. The fitted resistance ($R_{pc}$) from the arcs mostly attributed to the resistance at Au/HTM interface, because the HTM formed very thin overlayer (**Figure S6**†) in this study and the resistance of it is too small to resolve.[37] Therefore, the total series resistance of the devices can be calculated as $R_{series} = R_s + R_{pc}$, which has a serious effect on *FF* (**Table S1**†). As a consequence, DR3TBDTT+Li+tBP based device with the largest $R_{series}$ had the lowest *FF*, and DR3TBDTT+PDMS based device achieved the highest *FF* of 0.60 with the smallest $R_{series}$ of only 4.1 $\Omega \cdot cm^2$. The $R_{series}$ calculated from EIS matched the series resistance calculated from the *J-V* curve ($R_{series}^{\#}$) well and had a contrary tendency of *FF* (**Figure 3e**). A big interface resistance derived from the partial bareness of the perovskite, leading to a direct contact of perovkite and Au.[38] A full coverage of HTM on the perovskite layer is advantageous to fabricate an efficient device with a high *FF*. Therefore, a optimized hole transporting layer (HTL) should be a continuous, uniform film with the minimum thickness on top of the perovskite, consisting with the conclusions made by A. Dualeh et al.[37]

Li-TFSI in our study failed to enhance device performances, likely stemmed from two effects. Firstly, the introduction of Li-TFSI accompanying with its polar solvent into the solution of DR3TBDTT led to a reduced coverage on the perovskite resulting in low *FF* and PCE. Secondly, the thickness of HTL using conventional spiro-MeOTAD in devices usually needs to reach more than 140 nm, so the ion salt is essential to assist the hole transporting in such a thick film due to the poor pristine mobility of spiro-MeOTAD.[23,26,37] In our case, the thin capping layer of DR3TBDTT with higher hole mobility as its analogs as reported[31,32] had no need of the ion additive.

To define the role of PDMS, a device exclusively using PDMS to replace the HTM was fabricated and the performance of such device was as poor as the device without any HTM (**Figure S7**†). Moreover, DR3TBDTT with a higher content of PDMS exhibited an abnormal *J-V* curve demonstrating a huge resistance in the device derived from the excess addition of insulated PDMS. Besides, the XRD results revealed no obvious difference of molecule packing between the DR3TBDTT film and DR3TBDTT+PDMS film (**Figure S8**†). To sum up, the role of insulated PDMS was limited as a flow agent, who assisted the formation of a continuous, uniform and thin HTL, resulting in an significant enhancement of device performance.

All the devices exhibited good stabilities when stored under a relative low humidity of ~20% (**Figure S9**†). After 13 days of aging, the PCEs of spiro-MeOTAD+Li+tBP and DR3TBDTT+Li+tBP based devices decreased from 8.3% to 7.7% and 3.3% to 3.1%, respectively, with a ~6% reduction relative to the initial PCEs. While the performance decreased slightly from 8.3% to 8.1% for DR3TBDTT+PDMS based device (~2% reduction) and didn't decline for DR3TBDTT based device. However, when the devices of different HTMs were stored in a high relative humidity above 50%, the differences of device stability can be observed obviously (**Figure 4a**). Perovskite in devices containing Li-TFSI totally decomposed from dark brown to yellow after 3 days, with a sharp decline of PCE from 3.7% to 0.9% and 8.9% to 3.7% for DR3TBDTT+Li+tBP and spiro-MeOTAD+Li+tBP based device, respectively (**Figure S10**†). On the other hand, the perovskite in devices using DR3TBDTT and DR3TBDTT+PDMS still appeared dark brown, with the PCE changing from 4.9% to 4.4% and 8.8% to 8.0%, respectively, representing a superior stability. The obvious difference of device stability resulted from greatly different hydrophobicity of the HTL (**Figure 4b**). DR3TBDTT film showed a very big water contact angles of 107.4°, so that the hydrophobic HTLs can efficiently prevent the water penetration into the perovskite layer.[21] With the addition of PDMS, the angle declined slightly to 99.5°, still much bigger than that of spiro-MeOTAD+Li+tBP film. Both films containing Li-TFSI showed the smaller water contact angles around 80°, revealing a increased affinity of water caused by Li-TFSI. Such hydroscopic ion additives should be avoided in practical applications for perovskite solar cells due to its negative influence on device stability.

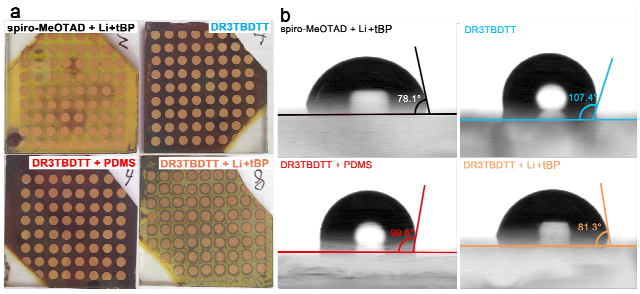


**Figure 4.** a) Devices exposured to a relative humidity >50% in air for 3 days at room temperature without encapsulation under illumination. b) Water contact angles of each HTM films on a glass substrate.

In summary, the hole transporting material DR3TBDTT was successfully synthesized with a well-matched HOMO energy level of 5.39 eV and excellent hydrophobicity for planar perovskite solar cells. By the addition of PDMS, a continuous thin capping layer on perovskite was formed as the HTL. Highest PCE for devices using DR3TBDTT+PDMS as the HTM achieved 8.8% without the addition of Li-TFSI, comparable to 8.9% obtained from spiro-MeOTAD+Li+tBP. However, the introduction of Li-TFSI into the HTMs led to decreased device stability due to the hydroscopicity of the ion additives. HTL composed of hydrophobic DR3TBDTT can efficiently protect the perovskite layer from moisture, so that the devices exhibited excellent stability. This work provides an efficient candidate of ion additive-free HTMs for highly stable perovskite solar cells.

We acknowledge the financial support from the National Natural Science Foundation of China (61177020 and 11121091) and the National Basic Research Program of China (2013CB328700). The authors are thankful to Mr. Xiao Yu and Prof. Dechun Zou in the College of Chemistry and Molecular Engineering of Peking University for their kind help in the assistance in the electrochemical impedance measurements.

## Notes and references

[a] State Key Laboratory for Mesoscopic Physics and Department of Physics, Peking University, Beijing 100871, China
[b] New Display Device and System Integration Collaborative Innovation Center of the West Coast of the Taiwan Strait，Fuzhou 350002, China

†Electronic Supplementary Information (ESI) available: Experimental details; Physical properties of DR3TBDTT; EDS; Absorption spectra; Stability of devices; Repeatability of devices; Device Performance; EIS fitting results. See DOI: 10.1039/c000000x/

1 A. Kojima, K. Teshima, Y. Shirai and T. Miyasaka, *J. Am. Chem. Soc.,* 2009, 131, 6050.
2 H.-S. Kim, C.-R. Lee, J.-H. Im, K.-B. Lee, T. Moehl, A. Marchioro, S.-J. Moon, R. Humphry-Baker, J.-H. Yum, J. E. Moser, M. Gräztel and N.-G. Park, *Sci. Rep.,* 2012, **2,** 591.
3 M. M. Lee, J. Teuscher, T. Miyasaka, T. N. Murakami and H. J. Snaith, *Science,* 2012, **338,** 643.
4 Q. Chen, H. Zhou, Z. Hong, S. Luo, H.-S. Duan, H.-H. Wang, Y. Liu, G. Li and Y. Yang, *J. Am. Chem. Soc.,* 2014, **136,** 622.
5 N. Pellet, P. Gao, G. Gregori, T.-Y.Yang, M. K. Nazeeruddin, J. Maier and M. Gräztel, *Angew. Chem. Int. Ed.,* 2014, **53,** 3151-3157.
6 H.-S. Kim, S. H. Im and N.-G. Park, *J. Phys. Chem. C,* 2014, **118,** 5615.
7 H. J. Snaith, *J. Phys. Chem. Lett.*, 2013, **4,** 3623.
8 J. Burschka, N. Pellet, S.-J. Moon, R. Humphry-Baker, P. Gao, M. K. Nazeeruddin and M. Gräztel, *Nature,* 2013, **499,** 316.
9 D. Liu and T. L. Kelly, *Nat. Photonics*, 2014, **8,** 133.
10 J. T. Wang, J. M. Ball, E. M. Barea, A. Abate, J. A. Alexander-Webber, J. Huang, M. Saliba, I. Mora-Sero, J. Bisquert, H. J. Snaith and R. J. Nicholas, *Nano Lett.,* 2014, **14,** 724.
11 K. Wojciechowski, M. Saliba, T. Leijtens, A. Abate and H. J. Snaith, *Energy Environ. Sci.,* 2014, **7,** 1142.
12 M. Liu, M. B. Johnston and H. J. Snaith, *Nature,* 2013, **501,** 395.
13 N. J. Jeon, H. G. Lee, Y. C. Kim, J. Seo, J. H. Noh, J. Lee and S. I. Seok, *J. Am. Chem. Soc.,* 2014, **136,** 7837.
14. A. Krishna, D. Sabba, H. Li, J. Yin, P. P. Boix, C. Soci, S. G. Mhaisalkar and A. C. Grimsdale, *Chem. Sci.,* 2014, **5,** 2702.
15. T. Krishnamoothy, F. Kunwu, P. P. Boix, H. Li, T. M. Koh, W. L. Leong, S. Powar, A. Grimsdale, M. Gräztel, N. Mathews and S. G. Mhaisalkar, *J. Mater. Chem. A,* 2014, **2,** 6305.
16. H. Li, K. Fu, A. Hagfeldt, M. Gräztel, S. G. Mhaisalkar and A. C. Grimsdale, *Angew. Chem. Int. Ed.,* 2014, **53,** 4085.
17. N. J. Jeon, J. Lee, J. H. Noh, M. K. Nazeeruddin, M. Gräztel and S. I. Seok, *J. Am. Chem. Soc.,* 2013, **135,** 19087.
18. J. Wang, S. Wang, X. Li, L. Zhu, Q. Meng, Y. Xiao and D. Li, *Chem. Commun.,* 2014, **50,** 5829.
19. S. Lv, L. Han, J. Xiao, L. Zhu, J. Shi, H. Wei, Y. Xu, J. Dong, X. Xu, D. Li, S. Wang, Y. Luo, Q. Meng and X. Li, *Chem. Commun.,* 2014, **50,** 6931.
20. J. H. Heo, S. H. Im, J. H. Noh, T. N. Mandal, C.-S. Lim, J. A. Chang, Y. H. Lee, H.-j. Kim, A. Sarkar, M. K. Nazeeruddin, M. Gräztel and S. I. Seok, *Nat. Photonics*, 2013, **7,** 486.
21. Y. S. Kwon, J. Lim, H.-J. Yun, Y.-H. Kim and T. Park, *Energy Environ. Sci.,* 2014, **7,** 1454.
22. H. Chen, X. Pan, W. Liu, M. Cai, D. Kou, Z. Huo, X. Fang and S. Dai, *Chem. Commun.,* 2013, **49,** 7277.
23. H. J. Snaith and M. Gräztel, *Adv. Mater.,* 2007, **19,** 3643.
24. U. B. Cappel, T. Daeneke and U. Bach, *Nano Lett.,* 2012, **12,** 4925.
25. R. Schölin, M. H. Karlsson, S. K. Eriksson, H. Siegbahn, E. M. J. Johansson and H. Rensmo, *J. Phys. Chem. C,* 2012, **116,** 26300.
26. A. Abate, T. Leijtens, S. Pathak, J. Teuscher, R. Avolio, M. E. Errico, J. Kirkpatrik, J. M. Ball, P. Docampo, I. McPherson and H. J. Snaith, *Phys. Chem. Chem. Phys.,* 2013, **15,** 2572.
27. R. Katoh, M. Kasuya, S. Kodate, A. Furube, N. Fuke and N. Koide, *J. Phys. Chem. C,* 2009, **113,** 20738.
28. J. H. Noh, S. H. Im, J. H. Heo, T. N. Mandal and S. I. Seok, *Nano Lett.,* 2013, **13,** 1764.
29. P. Qin, S. Paek, M. I. Dar, N. Pellet, J. Ko, M. Gräztel and M. K. Nazeeruddin, *J. Am. Chem. Soc.,* 2014, **136,** 8516.
30. G. Niu, W. Li, F. Meng, L. Wang, H. Dong and Y. Qiu, *J. Mater. Chem. A,* 2014, **2,** 705.
31. J. Zhou, Y. Zuo, X. Wan, G. Long, Q. Zhang, W. Ni, Y. Liu, Z. Li, G. He, C. Li, B. Kan, M. Li and Y. Chen, *J. Am. Chem. Soc.,* 2013, **135,** 8484.
32. J. Zhou, X. Wan, Y. Liu, Y. Zuo, Z. Li, G. He, G. Long, W. Ni, C. Li, X. Su and Y. Chen, *J. Am. Chem. Soc.,* 2012, **134,** 16345.
33. Y. Liu, Y. Yang, C.-C. Chen, Q. Chen, L. Dou, Z. Hong, G. Li and Y. Yang, *Adv. Mater.,* 2013, **25,** 4657.
34. Y. Ma, L. Zheng, Y.-H. Chung, S. Chu, L. Xiao, Z. Chen, S. Wang, B. Qu, Q. Gong, Z. Wu and X. Hou, *Chem. Commun.,* 2014, DOI: 10.1039/C4CC01962H.
35. L. Zheng, Y. Ma, S. Chu, S. Wang, B. Qu, L. Xiao, Z. Chen, Q. Gong, Z. Wu and X. Hou, *Nanoscale,* 2014, **6,** 8171.
36. J. W. Du, in *Coatings Technology Handbook,* ed. A. A. Tracton, CRC Press, Boca Raton, FL, USA, 3rd edn., 2006, ch. 75.
37. A. Dualeh, T. Moehl, N. Tétreault, J. Teuscher, P. Gao, M. K. Nazeeruddin and M. Gräztel, *ACS Nano,* 2014, **8,** 362.
38. E. J. Juarez-Perez, M. Wuβler, F. Fabregat-Santiago, K. Lakus-Wollny, E. Mankel, T. Mayer, W. Jaegermann and I. Mora-Sero, *J. Phys. Chem. Lett.*, 2014, **5,** 680.
39. V. Gonzalez-Pedro, E. J. Juarez-Perez, W.-S. Arsyad, E. M. Barea, F. Fabregat-Santiago, I. Mora-Sero and J. Bisquert, *Nano Lett.,* 2014, **14,** 888.
40. H.-S. Kim, I. Mora-Sero, V. Gonzalez-Pedro, F. Fabregat-Santiago, E. J. Juarez-Perez, N.-G. Park and J. Bisquert, *Nat. Commun.,* 2013, **4,** 2242.
41. Y. Xu, J. Shi, S. Lv, L. Zhu, J. Dong, H. Wu, Y. Xiao, Y. Luo, S. Wang, D. Li, X. Li and Q. Meng, *ACS Appl. Mater. Interfaces,* 2014, ***6,*** 5651.



 

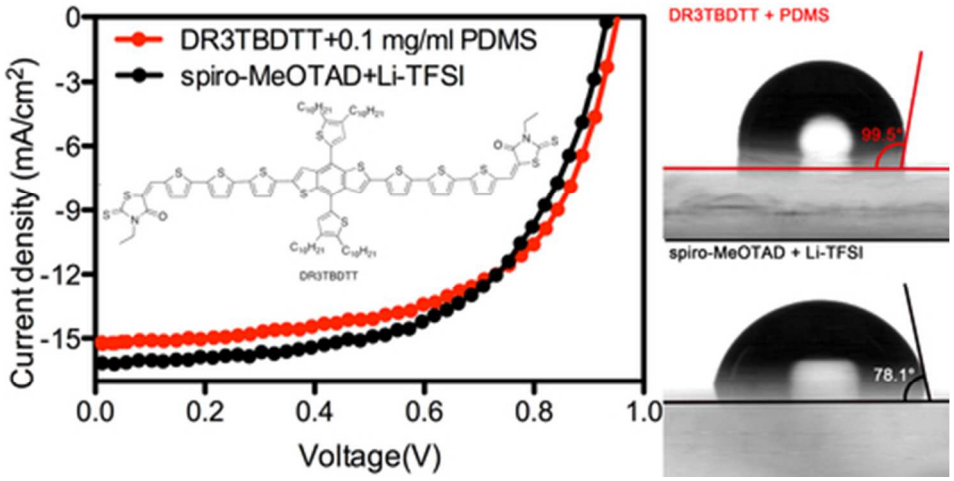


An oligothiophene derivative with highly hydrophobicity was synthesized and functioned as HTM for perovskite solar cells without ion additive, resulting in improved device stability than that using Li-TFSI doped spiro-MeOTAD.
39x19mm (300 x 300 DPI)